PARAMETRIC STUDY OF PERFORMANCE OF AIRCRAFT EQUIPPED WITH AIRBORNE REACTIVE AND FORWARD LOOKING SENSOR DURING MICROBURST ENCOUNTER INCLUDING RAINING EFFECT.

MM. Descatoire, F.(1), Guffond, D.(2), Huynh, H.T.(1)
Office National d'Etudes et de Recherches Aérospatiales (ONERA)
(1) Ecole de l'Air - BA 701 - 13661 Salon de Provence - France
(2) 29 Avenue de la Division Leclerc - 92320 Châtillon - France

Abstract

This paper presents a parametric study, through numerical simulation on performance of aircraft which were assumed to be equipped with fully automated guidance/control system, coupled with airborne windshear detection systems, when encountering windshear during low altitude manoeuvres.

Two kind of microbursts are recensed : dry microbursts which can occurred without any precipitation, and wet microbursts which are accompanied by heavy rains. In this last case, non stationary effect of wind on rain droplets can increase water concentration, particularly near the core of microburst, where local rain intensity can thus reaches ten times mean rain intensity at the outside of microburst.

Effect of rain intensity on performances of several typical aircraft models, with guidance/control system coupled with reactive windshear detection, is shown during take-off and landing phases.

Concerning dry microbursts, study also was performed with airborne forward looking system (FLS), based on Doppler lidar detection system, taking into account intensity and position of microburst along trajectories. Influence of forward-look distance on aircraft performance was also analysed. Thus in critical situation it was found that reactive or short range FLS (700m) did not provide enough safety for aircraft, and a minimum alert time between 20s and 30s was necessary to achieve a safer recovery trajectory.

Nomenclature

ALDF: Aircraft Landing Dynamic Facility
CFD: Computation Fluid Dynamic
FLS: Forward Looking System
ILS: Instrumented Landing System
GARTEUR: Group for Aeronautical Research and Technology in EURope.
XDB: position of the downburst along the flight path relative to the runway threshold or Lift-off point.
Cf: : concentration factor
dot : 0,25 degree deviation about nominal glide slope
D: aerodynamic drag
e_L : unit vector along the laser beam
F: windshear Hazard factor
Flaser: windshear FLS hazard factor
Fmax: maximum thrust (N)
m : aircraft mass (kg)
R_1 : rainfall rate coefficient
Rl : local rainfall rate (mm/hr)
R : rainfall rate outside the microburst (mm/hr)
tx : time-filtering parameter
T : total thrust
u_W : horizontal wind component (m/s)
V : airspeed
Vz : vertical inertial speed
$V_s = V_{stall}$: stall airspeed in steady horizontal flight
w_W: vertical wind component (m/s)
$V_{doppler}$: Doppler-derived velocity (m/s)
V_W :velocity of the particle at scanned location
V_L : velocity of the laser source (point L)
w : derivative relative to time of total height
ΔR : range grid or range bin interval along the laser beam
τ : engine response, time constant of a first filter order
γ_k : inertial flight path angle

Introduction

One of the most dangerous situations for an aircraft during low altitude manoeuvres, i.e. take-off or approach and landing, is caused by the presence of strong windshear associated with microburst phenomena. A microburst is a strong, localized downdraft that strikes the ground, providing winds which diverge radially from the impact point. An aircraft penetrating through the centre of a symmetric microburst will initially encounter an increasing headwind, followed by a strong downdraft and rapidly increasing tailwind. The effects of downdraft and increasing tailwind may exceed the performance capabilities of the aircraft, causing unavoidable accidents. In order to reduce the hazard of low-level windshears to aircraft operations, numerous studies were performed in various domain such as: better knowledge of atmospheric phenomena and their probability of occurrence [1] [2], development of airborne and ground-based windshear detection systems [3] [4], guidance and control systems [5], training and operating procedures [6].

Microburst can occurred without any precipitation (dry microbursts), or can be accompanied by heavy rains (wet microbursts). In this last case, non stationary effect of wind on rain drops can increase water concentration, particularly near the core of the microburst. The influence of heavy rains in performance of aircraft, when encountering wet

microburst were also performed, without taking into account the concentration effect [16].
The objective of this study is to contribute to the evaluation of the aircraft performance during windshear encounter, which a special emphasis on the rain effect. Minimum performance requirements for airborne forward looking systems (FLS) with several aircraft models were also investigated.
For this purpose, a complete non-real time numerical simulation was set up, simulating the behaviour of an aircraft which is assumed to be equipped with a fully automated flight control system during approach/landing and take-off phases. The paper describes first the models used in the numerical simulation: wet microburst, aircraft and performance in presence of rain, windshear detection systems and guidance strategies which are coupled with. The results of off-line numerical simulations are then presented with effect of several parameters during approach/landing and take-off phases.

Model descriptions

Aircraft models

For non real time simulation studies two types of aircraft models were used: a complete longitudinal generic aircraft model and a simplified model, call behaviour model .

Complete longitudinal generic aircraft model (A1).

This model represents the longitudinal motion of a generic twin-engined heavy transport aircraft, including a dynamic thrust response. It was developed within a work in an European cooperation program GARTEUR [7].
The system control used for the landing approach is composed with an auto-pilot or flight path controller for ILS tracking and an auto-throttle or airspeed controller. In the autopilot the true glide path deviation, height, vertical acceleration and pitch attitude are processed and the elevator and trim tab are adjusted accordingly. The thrust command is formed by the auto-throttle from airspeed deviation, longitudinal acceleration and pitch attitude.
In the go-around situation, the controller feeds back only the pitch angle deviation and pitch rate. A constant pitch angle is commanded and an angle of attack protection is included to avoid a stall.
In the take-off phase, a constant maximum power is applied and a pitch angle is commanded including the maximum angle of attack protection.

Behaviour model (A2, A3, A4)

The previous aircraft is common to aircraft which are involved in windshear accidents. It is possible to get responses to various windshear profiles. Nevertheless, this model did not permit to carry out parametric studies on performance such as the response to windshear encounter when aircraft characteristics need to be modified. A simplified model, designed as behaviour model, was developed. This behaviour type model can describe correctly the flight dynamic response of an aircraft equipped with its control and guidance system during landing approach, go-around, take-off phase, by taking into acount the guidance strategy and the automatic maximum angle of attack protection. This model has adjustable characteristics such as: maximum angle of attack, drag aerodynamic polar, short period mode, engine response model.
Three behaviour models were used and were defined as follow:
A2 is a three low by-pass ratio engines medium range transport aircraft;
A3 is a twin high by-pass ratio engines long range transport aircraft;
A4 is a four high by-pass ratio engines long range transport aircraft.
Table 1 and Table 2 give the landing and take-off weight and some characteristics in landing configuration respectively.

Windshear models

Since the interaction between aircraft and atmosphere was subject of investigation, both the mathematical model of the aircraft including subsystems and the wind model need to be compatible and have to properly consider the effects to be evaluated. Two windshear models were selected from the numerous model approaches for different applications with the understanding that :

- the model must provide realistic wind situations;
- the model must provide realistic rain concentration;
- the application of earth fixed stationary wind model is sufficient;
- simple structure, handling and acceptable computation time are to be obtained.

To investigate the rain concentration effect a CFD code developed by ONERA was able to model microburst which are accompanied by heavy rains.
To investigate the benefit of FLS, the approach of Oseguera and Bowles for modelling dry Downburst phenomena was chosen [8].

Downburst model used for the FLS study

It represents a simple analytical downburst developed for real-time and off-line investigations. The model represents an axi-symmetric stagnation point flow which is assumed as time invariant. The flow is incompressible and satisfies the mass continuity equation. The effects of viscosity were parameterized explicitly by using a pair of shaping functions that gave profiles for vertical and radial velocity matching the Terminal Area Simulation System (TASS) [9] velocity profiles which are assumed to be close to real-world measurement.

Microburst model used for the raining effect study

It is advisable to modelize the velocity field of a microburst which impinges on the ground taking into

acount the dynamic of the rain drops. The aerodynamic flow field and rain drops trajectories computed by ONERA are described in [10] [11].

In a first step, a numerical simulation was set up by solving the non stationary three dimensional Navier-Stokes equation of a non viscous incompressible flow. In a new version, in order to have a better drawing to the real physical phenomena, air density variations and gravity forces relative to the altitude were taking into acount. The microburst was modelized in a parallelepiped of 8km wide and 5km high. Resolution of the Navier Stokes equation gaves at any time and any space location the speed when the microburst was spreading out (Fig 1). This figure represents the wind vectors and their modulus for the half part of the flow field at several instant (t=800 s, 1000 s, 1200 s) from the symmetry axis to 1500m in width and from the ground to 600m in height.

Computation of the rain drops trajectories was based on the following assumptions:

- the presence of rain drops did not modify the aerodynamic flow field;
- drops have spherical shape and a constant diameter:1 mm;
- the only forces affecting the motion were the constant gravity and the drag forces due to velocity differences between drops and the surroundings air.

As the flow was non stationary, the aerodynamic flowfield was computed with a time integration step of 2 s.

Concentration factor computation

The local concentration in rain drops was calculated in the microburst by this way: as we used an axisymmetric model for the microburst, four drops at a given time t0 delimited a volume equal to $r_{t0}\ S_{t0}$ (with S_{t0} being the area delimited by the four drops and r_{t0} the distance between the microburst axis and the centre of this area). At a further time t1, the same four drops delimited a volume $r_{t1}\ S_{t1}$. Assuming that all the drops inside the first volume remained inside the second one, a concentration factor Cf can be defined as:

$$Cf = rt_0\ St_0 / rt_1\ St_1$$

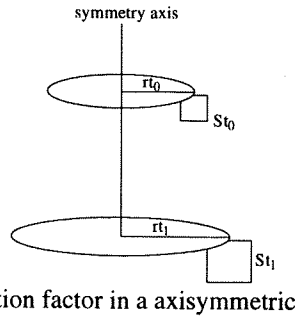

Concentration factor in a axisymmetric flow field

The airfoil performance degradation produced by rainfall was given versus the rainfall intensity (in mm/hr). This intensity at the ground level is proportional to the liquid water content multiplied by the rainfall velocity. In a similar way, the rainfall intensity along the plane trajectory will be considered to be proportional to the product of the concentration factor (Cf) by the local rain drop velocity (Ve). The rainfall rate coefficient is defined as

$$R_1 = \frac{Cf.Ve}{Cf_\infty . Ve_\infty}$$

The product of the rainfall rate coefficient (R_1) by the rainfall rate outside the microburst (R) gives the local rainfall rate which was used as an input data to evaluate the aero-dynamic performance penalty:

$$Rl = R_1 . R$$

Values of R (mm/hr) will be further discussed.

The rainfall rate coefficients R_1 corresponding to the time t=800s , 1000s, 1200s are shown in Fig 2. A large area of rainfall concentration moving towards the ground and then dispersing can be observed. The rainfall rate coefficient in the core of the microburst at time t=800s can reach the value of 10 .

The characteristics of heavy rain.

The heavy rainfall rate have been measured at the ground [13] and also in flight [14]. High-intensity and short-duration rainfall characteristics associated with thunderstorms were also collected [15]. The maximum volume of rain accumulated in one minute time interval was equivalent to a rainfall rate of 1830 mm/hr [13] whereas in one second [15] the maximum rainfall rate measured was 720 mm/hr. The upper boundary for airborne measurements [14] corresponded to approximately 2920 mm/hr. In the numerical simulations three values of rainfall rate outside the microburst at the ground (R) were chosen from the above results [13][15]: R = 12.5 , 50, 150 mm/hr corresponding to a moderate, heavy, very heavy rain respectively. The high rain concentrations of the wet microburst model would bring the aircraft to encounter local rainfall rate (Rl) up to 1500mm/hr.

Effects of heavy rain on aerodynamic model

Results from a broad NASA research program [16][17] to obtain fundamental aerodynamic information regarding the effect of heavy rain on airplane performance were used in this study. Based on the comparisons available between the limited large-scale results obtained on the ALDF Rain Simulation System and wind tunnel results [16], rain scale effects are not large and wind-tunnel results can be used to predict large-scale heavy rain effects. The results of these tests shown that heavy rain can significantly increase drag as well as decrease lift and stall angle of attack. The tests also showed that :

- the cruise configuration was less sensitive than the high lift configuration to rain environment;
- the transition times for the wing to achieve a steady state condition encountering simulated heavy rain is less than two to three seconds in most cases [18].

The aerodynamic effect of heavy rain on a full configuration airplane was investigated by Vicroy [16] who integrated the wind tunnel section data across the wing planform. The wet airplane aerodynamics could be

approximated by modeling the change in the lift and drag with liquid water content from the integrated results, and apply this perturbation model to the dry baseline aerodynamic model. Within the framework of this study, the perturbation model to the dry baseline aerodynamic model was simplified and consisted in applying the ALDF airfoils results to the maximum lift and stall angle of attack and the integration results to the drag. The decrease of the maximum lift is more significant in landing configuration than in take-off configuration but the loss of lift to drag ratio due to heavy rain effect is more sensitive in take-off configuration than in landing configuration (Fig 3) .

Heavy Rain Effect on Climb Performance

The specific excess power depends on the maximum thrust and the lift to drag ratio. The maximum specific excess power is defined by:

$$\frac{W}{V} = \frac{Fmax}{m.g} - \frac{1}{f}$$

which is equivalent to, in absence of any atmospheric perturbation:

$$\frac{W}{V} = \frac{Vz}{V} - \frac{\dot{V}}{g}$$

The specific excess power gives the acceleration capability in an horizontal flight path or the climb performance at a constant airspeed. Climb performance depends on the type of aircraft (twin, three, four engines powered aircraft) and on configuration as shown Fig 4 and Fig 5. Loss of climb performances due to rainfall rate can also be observed. The specific excess power of the A1 aircraft model under increasing rainfall rate up to 1000mm/hr for landing configuration is shown in Fig 6. Rainfall rate reduces the specific excess power which is less dependent of airspeed for this configuration. This is also true for the take-off configuration.

Windshear detection systems model

Two classes of airborne windshear detection systems can be distinguished:

The « reactive » windshear detection systems, based upon existing air data and inertial sensors, and which are able to identify the presence of windshear once the phenomenon is encountered and which provide suitable informations (warning, flight guidance, displays) to the pilot to cope with the danger.

The « forward-looking » or « predictive » windshear detection systems (FLS) which are able to sense windshear conditions before the phenomenon is encountered and which provide suitable informations to the pilot, well in advance, to improve aircraft safety.

The key to the design of an airborne windshear detection system is the definition of a hazard criteria.

Hazard factor for reactive system

The F-factor is a hazard criteria which directly represents the airspeed variation due to a wind variation as can be expressed by the dynamic equation :

$$\frac{dv}{dt} = g\left(\frac{T-D}{m} - \gamma_k - F\right) \quad (1)$$

where the F-factor is defined as follow:

$$F = \frac{\dot{u}_W}{g} - \frac{W_W}{v} \quad (2)$$

One of the boundary curves, as suggested by the TSO-C117 [19], for the determination of threshold values is used for reactive detection system. The average F-factor is defined in the TSO-C117 as:

$$F_{av}(t) = \frac{1}{tx}\int_{t-tx}^{tx} F(\tau)d\tau \quad (3)$$

The level of F_{av} which triggers the alert depends on the choice of tx. In this study tx was fixed equal to 5s.

Hazard factor for forward looking system (FLS)

Several technologies are under development for forward-looking windshear detection: Doppler radar, IR radiometer, Doppler lidar. The most promising sensor seems to be the airborne pulsed Doppler weather radar, under the presumption that the problems of ground clutter rejection and detection of « dry » windshear are solved. The major disadvantage is that this system cannot detect very dry microburst which a laser can. Fig 7 [12] compares the domain of application of airborne radar and lidar. In this study a very simple functional model of airborne forward looking sensor has been based on the Doppler-lidar type, but the results could be extended without major difficulty to a Doppler-radar system. The model provided an estimate of the Doppler derived wind vector from a minimum laser range (Rmin) to a maximum scanning range (Rmax) as shown in Fig 8. The minimum range depends upon the laser pulse width and the times it takes to switch from transmitting to receiving status. The maximum range depends on others system characteristics and is limited by precipitation. The Doppler velocity is given by:

$$V_{doppler} = (\vec{V}_w - \vec{V}_L).\vec{e}_L \quad (4)$$

The beam was assumed to be stabilized along the inertial flight angle of the aircraft and there was no scanning in azimuth.

By pulsing the laser, then at varying distance from close to the aircraft to Rmax, the Doppler lidar can thus provide instantaneously a set of discrete measurements of Doppler velocity from a minimum to a maximum range along the beam. Several data processing techniques can be then applied to the Doppler-lidar measurements, in order to provide a value of severity factor, based upon F-factor given in Eq (2), or upon other hazard criteria [7]. This study adopted one data processing technique, noted by Flaser, which relied upon a time-filtering on maximum F factor values derived from Doppler-lidar measurements and which provided the best result in terms of a timely detection of windshear severity [7].

Nevertheless, it can be noticed that a FLS, based upon a Doppler-lidar system, as described above, did not provide a complete measure of the hazard criterion F-factor in Eq (2). Indeed, by assuming that the laser beam scans along a

horizontal axis, it can be shown that the Doppler-lidar measurements provide only the first term of F-factor.

Alert levels

Several alert levels were first defined, according to [19] in terms of hazard F-factors (Fav for the reactive system, Flaser for the predictive system) and the corresponding threshold. One can distinguish the following levels:

level (color)	Fav , Flaser
1 (green)	F. $\leq$ 0.04
2 (yellow)	0.04 < F. $\leq$ 0.1
3 (amber)	0.1 < F. $\leq$ 0.205
4 (red)	F. > 0.205

The proposed guidance strategies can be executed manually or automatically so as to enable the crossing of a windfield with a maximum level of safety, taking into account both reactive and predictive systems. Otherwise guidance strategies must have the following properties:

- simplicity of execution
- robustness against windshear fields
- high level of flight safety

Guidance strategies for reactive system

Penetrating approach/landing strategy

The guidance strategy consist of adding a constant speed increment (ΔV) to the final approach speed. If the Fav factor entered the «yellow» zone, an increment of 5kts would be added to the controlled reference airspeed. If this factor continued to increase such that it entered into the « amber »zone, another 15kts would be added to the controlled airspeed, which corresponded to a total speed increase of 20kts. If this still was not sufficient to cope with the windshear and the «red» zone was entered, the go-around mode would be triggered. Notice that with the reactive system there was no decision logic to reduce the airspeed when exiting the windshear.

Go-around strategy

The go-around guidance consisted of applying full thrust and commanding a constant pitch value. Nevertheless, when encountering a strong windshear, the go-around controller automatically executed an angle of attack protection by reducing the pitch angle, if necessary.

Take-off strategy

It consisted of reducing the pitch angle during the first phase of a windshear encounter in order to increase the airspeed, then to increase the pitch to a higher value than the nominal value, in order to avoid a loss of altitude during windshear penetration. The decision for this higher pitch was given if the actual vertical speed exceeded a preset vertical inertial speed. The maximum angle of attack protection was also include in the strategy.

Guidance strategy for the FLS

The F-factors derived from the laser informations were tested with the same hazard levels as defined for the reactive system, with a same time-filtering equal to 5s.
In case of penetrating landing, a speed increase up to a maximum of 20 kts above the reference speed was used when a FLS or a reactive system indicate entering the microburst. A speed reduction, down to reference approach speed, was adopted with a FLS in combination with a reactive system at the exit of the microburst.
The decision to initiate go-around was provided by «red alert» associated with Flaser. This decision was used for a forward looking sensor of the Doppler-lidar type in the worst conditions, i.e. with reduced range (less than 2000 m) and small scanning space volume. The escape manoeuver was limited in this study to the vertical plane only without lateral escape.
At take-off a FLS could be used during the ground-roll phase in order to abort a take-off before decision speed V1. This segment is not investigated in this study. The guidance law for take-off with a FLS was a pitch attitude guidance law with stall protection.

Results of numerical simulation

General asumptions

The ground-roll at take-off and flare at landing were not simulated. The approach/landing simulations have been performed as follows:

- penetrating landing with go-around decision inhibited;
- aborted landing where the go-around initiation is provided by the windshear detection logic only.

Aircraft performance in presence of wet microbursts

The analysis was performed on aircraft coupled with a reactive windshear detection system only, including the speed increment strategy and the microburst model was generated by CFD code with several dispersal time.

Generic aircraft response during a penetrating approach

The aircraft was initialized far away from the centre of the downburst, on the nominal glide slope with nominal airspeed for approach/landing.
In approach/landing simulations, the origin of the reference axes (x-h) was located at the runway threshold. The final conditions are given as follows (see Table 2) :

- either a horizontal distance X_0 when the altitude h_f = 15 m was crossed (a negative value of X_0 correspond to a position before the runway threshold) ;
- or the altitude of the aircraft when the x-axis was reached.

The simulations were performed in the following conditions:

- two locations (XDB) of the symmetry axis of the microburst to the runway threshold;

- three dispersal time (t=800s, 1000s, 1200s) of the microburst.

One example of a penetrating approach is shown in Fig 9. This non stabilized approach should lead to a go-around procedure triggered by a 0.4 value of the F_{av} factor.
The microburst dispersal effect in the considered time step, both XDB locations, did not permit to execute a safety approach, as shown in Table 3.
The worst situation happened when the microburst was located closed to the runway (1500 m) because the aircraft penetrated at low altitude a strong horizontal windshear. In these cases the hazard F factor could reach 0.47. The windfield structures showed:

- a «common» horizontal windhear profile at time t=800s (see wind profile on Fig 10);
- a «more complex» horizontal and vertical wind profiles (Fig 9) at time t=1000s, 1200s which provided less severe gradients than the t=800s wind profile.

In the case where the dry microburst (t=1000s) was located at 3000m (Fig 9) the trajectory about the nominal flight path was altered and the limits of +/-1dot were exceeded but final conditions (sink rate and ground speed) to initiate the flare were acceptable for a good landing. In numerical simulations, it was possible to separate the windfield and raining effects. Simulations of penetrating approach have been performed with a wet microburst by applying several R parameters and also without windfield profiles but with only rain concentration profile (Fig 9). Local rainfall rate reached 800mm/hr in the core of the wet microburst for R=150mm/hr, and a maximum thrust was used to overcome the windshear and rain. At the end of the windshear overshooting the glide path did not permit to recapture the nominal trajectory. With the rain only, it was possible to perform a safe approach/landing, i.e., glide deviations are less than one dot, angle of attack deviations less than 4°, airspeed deviation less than 10%.

Aborted approach

The go-around mode was only triggered by the « red » windshear alert. At time dispersal t=800s, the flight path was still descending after the go-around mode was engaged. Angle of attack increased up to 17°, airspeed decreased to the stall airspeed (Fig 10). With a complex windshear profile due to dispersal time effect (t=1000s, 1200s), the go-around mode was triggered more early and the descending phase under the glide path was reduced. The airspeed was maintained above $1.1Vs_1$, the maximum angle of attack reached 15°. The minimum altitude during the go-around procedure mainly depends on the microburst location as shown results plotted in Fig 11. High rainfall rate which occurred in the core of the microburst reduced maximum lift coefficient. The effect was a lower minimum altitude due to rainfall. In case of heavy rainfall rate (R=150mm/hr) additional altitude loss was about 45m when the microburst was located at 3000m. In spite of the increase of drag due to rainfall, the airspeed never decreased below the stall airspeed and the angle of attack did not reach the stall angle. The lowest altitude during go-around was reached when the microburst (t=800s) was located near the runway threshold (1500m) with heavy rainfall rate (R=150mm/hr). In this case local rainfall rate along the flight path reached 1500mm/hr.

Parametric aircraft model results

Results analysis were focussed on the aborted landing simulate with the severe microburst (t=800s). The angle of attack decreased (headwind effect) before triggering the go-around mode, and then increased when crossing the shear. When the go-around mode was engaged, a full thrust was applied and the angle of attack moved moderately due to the wind components but the pitch auto-pilot might command to decrease the pitch angle in order to avoid the aircraft from stalling. At the end of the windshear, the angle of attack decreased, the pitch attitude led towards the climb at constant speed value.
The minimum altitude which were reached during aborted landing were closed for all aircraft models (Table 4). Without rainfall these values mainly depended on time engine response because the go-around procedure was engaged at the same position on the glide path. One can notice a more critical situation for the A3 and A4 models when the microburst was located near the runway threshold.
Additional altitude loss due to moderate rainfall (R=50mm/hr) was equivalent for all aircraft models whereas under very heavy rainfall (R=150mm/hr) the A2 model was less sensitive (Fig 12). In this last case, stall hazard occurred on the A3 and A4 types, maximum angle of attack tended to the stall angle and airspeed briefly decreased below the stall airspeed. A2 model had a lower angle of attack in approach and a higher Vref/Vs in approach than A3, A4 models (Table 2).

Take-off

In the take-off simulations, the origin of the reference axes (x-h) was located at the point where all the simulations were initialized, i.e. at altitude $h_0 = 15$ m.
Simulations were performed with the microburst windfield at t=800s.

Generic aircraft response during microburst encounter.

After lift-off, the F factor is first negative (energy gain), become positive when crossing the shear (energy loss due to horizontal windshear and downdraft), finaly negative at the exit of the windshear. Under dry or wet severe windshear conditions a descent phase may occur during take-off (Fig 14). The altitude margin (dh) (defined as shown in Fig 14) related to a defined minimum path slope of 3,3% decreased when the microburst was close to the lift-off point. In rainfall condition climb performance were decreased, then altitude margin was reduced (Fig 13). With this aircraft model a descending flight path was observed

under heavy rain condition (R=150mm/hr) with the microburst located at 1000m but the altitude margin remained positive (Fig 14). On this figure one can notice separated effects of the atmospheric perturbation where local rainfall rate reach 1000mm/hr. The effect of the only rainfall profile was much less important than the effect of the wind profile.

Parametric aircraft model results

Flight path trajectories obtained with the dry microburst located at 1000m showed that all aircraft models were able to maintain a positive altitude margin (dh) but were forced to a descent phase (Fig 15). As climb performances decreased with rainfall rates (Fig 4), rainfall provided additional altitude losses. Fig 16 shown the whole aircraft results.

Comparison between reactive and forward looking systems

The results obtained are shown for an aircraft equipped with different systems:

- Basic automatic pilot (basic A.P)
- Reactive system with speed increment strategy (reactive system)
- FLS with speed increment strategy (FLS)

An extreme downburst can demonstrate the interest of forward-looking windshear detection system to improve aircraft safety. The main characteristics of the analytical downburst model, as describe above [9], were chosen in order to create a severe downburst [7].

The look ahead distance parameter has been determined by the time delay of 10s, 20s, 30s at nominal approach speed coresponding to 700m (short range), 1400m (medium range), 2100m (long range).

Penetrating approach and landing

Fig 17 present the response of a generic aircraft model (A1) during a penetrating landing phase, with a microburst centered at 4000 m from the runway threshold. With the FLS it was found that increasing speed early enough the stall margin was improved and the aircraft could reach the runway threshold in good conditions. The trajectory was strongly altered and the limits ± 1 dot were exceeded as well as the limit V/Vs = 1.1. At the center of the microburst the thrust was at its maximum value when it was completely reduced in the tailwind leg. The conditions found at the runway threshold in function of forward looking distance were not acceptable for the short range (700 m) whereas for longer range (1400 m and 2100 m), the aircraft reached the runway threshold in good conditions for the flare and landing.

For this microburst windfield, the position along the flight path relative to the touch-down point has a large influence on the aircraft flight safety. Simulations performed with a FLS (1400 m range and guidance strategy based on Flaser) indicates critical locations of the microburst which lead to a crash before the threshold (3600m < XDB < 2500m) or an overshooting (XDB < 2500m).

Aborted approach

Guidance strategies associated with FLS with go-around decision were first evaluated with the generic aircraft model (A1) in a strong microburst windfield located at 4000m and then 2500 m from the runway threshold. The following can be noted (Fig 18, 19):

- increasing the speed before actually entering the shear may increase the survivability of the aircraft;
- the earlier the speed is increased, the better the energy of the aircraft will be;
- the advantage of a FLS compared to a reactive system allows the go-around to be early enough to enhance the aircraft's flight path safety.

One can see that in a critical windshear encounter the suggested guidance strategy with a FLS allowing a 20 s alert time (1400 m range) increased aircraft safety when crossing (Fig 20). The trajectory of the aircraft remained above the nominal descent flight path. With a look-ahead distance of a shorter range (700 m) the results were similar to those obtained with a reactive system, and led to a crash during the go-around procedure.

With the A4 model, the minimum altitude after triggering the go-around procedure versus the downburst position and the systems are plotted on Fig 21. When the downburst was centered far away to the runway threshold (5km), the look-ahead distance had smaller effects on minimum altitude reached after go-around initiation, than when it was centered closer (2.5km).

This was caused by the Flaser factor which underestimated the windshear hazard. Therefore the go-around mode might be triggered by the reactive system, even if the aircraft was equipped with a FLS. Aircraft parametric study (Fig 22) has shown that a 2100m detection range was necessary to trigger a go-around early enough in order to obtain a safe recovery.

Take-off

The FLS allowed to minimize deviations from the nominal climb trajectory by decreasing the pitch attitude before entering the shear so that the airspeed remained at a high value (Fig 23). This energy was used when the aircraft had to fly at high angle of attack for crossing the shear in order to avoid a descending phase. Reactive and FLS systems were efficient when downburst was located far away from the origin of x-axis (2000 m). In other situations (Fig 24), the guidance strategy associated with a windshear detection system (reactive or FLS) did not provide better results in terms of altitude margin (dh) than those obtained with a basic auto-pilot.

The behaviour of aircraft relied more on its performance than on the applied guidance strategy and windshear detection systems as shown Fig 25. Aircraft parametric study showed that an aircraft with good climb performance (A3 model) was able to cope with severe downburst in safety using a the FLS, with at least a 1400m look ahead distance. Result obtained with a shorter range was similar

to the reactive system because the command to decrease the pitch angle occurred later, when entering the shear.

Conclusions

A parametric study on aircraft performance during windshear encounter at low-altitude manoeuvres, i.e. approach/landing and take off, is presented in this paper with a special emphasis on wet microburst and minimum requirements for airborne forward-looking sensors. A numerical simulation was set up, taking account several aircraft models, equipped with a fully automated guidance/control system coupled with windshear detection systems, and microburst model.

Wet microburst wind profile was obtained through a numerical fluid dynamic computation code which took into account non-stationary effects of wind and precipitation. Numerical integration of microburst simulation indicated the existence of local high rain intensity within the core, caused by non stationary effect of wind on rain droplets and which could reach ten times the rain intensity outside the microburst.

Off-line simulation of aircraft behaviour, with guidance strategy coupled with a reactive windshear detection system showed that the influence of rain was much less important than wind gradients caused by microburst. Nevertheless, as rain reduced the aerodynamic performance of aircraft (maximum angle of attack, drag), the presence of rain increased the degradation on aircraft performance during windshear encounters.

Minimum requirements for look-ahead distance associated with forward-looking system (FLS) based upon a Doppler-lidar sensor were evaluated in a similar parametric study, using an analytical strong downburst model verifying mass continuity equation. Simulation results indicated that the most important parameter was the instant where guidance strategy was applied. It was also found that this previous alert time was strongly dependent on the characteristics of FLS (look-ahead distance), the severity of the shears, and the thresholds which were used in the guidance strategy. It was found that a minimum alert time between 20s and 30s was necessary to obtain a safer recovery trajectory, with a fully automated guidance and control system during approach/landing. This minimum alert-time was longer for a quadri-engines aircraft model (30s), than for twin-engine aircraft model (20s).

Take-off were simulated, after lift-off phase only, and the results indicated that the performance of the aircraft, as suspected, were less dependent on the guidance strategy coupled with the FLS, than on the severity of the microburst.

References

[1] Bowles R. L. Frost W
Wind Shear/Turbulence Inputs to Flight Simulation and System Certification
NASA Conference publication 2474, (1987)

[2] Haverdings H., et al.
Windshear occurences in Europe. Some annotated cases and inquiry into a windshear database
Garteur TP-086, (Revised edition 1996)

[3] Bowles R.L
Reducing windshear risk through airborne systems technology.
ICAS-90-1.9.3. Stockholm, (1990)

[4] Bracalente E.M., Britt C.I. and Jones W.R.
Airborne Doppler radar detection of low-altitude windshear
Journal of Aircraft Vol 27 n°2, (Feb.1990)

[5] Miele A., et al.
Acceleration, Gamma and Theta guidance for abort landing in a windshear
Journal of Guidance, Navigation and control.Vol 12, (1989)

[6] Hinton D.A., Oseguera R.M.
Microburst avoidance crew procedures for forward-look sensor equipped aircraft
AIAA 93-3942 Monterey, CA. (1993)

[7] Huynh T., et al.
Performance evaluation of airborne reactive and forward looking windshear detection systems on a simulated aircraft
Garteur TP-092, 1996 (to be published)

[8] Oseguera R.M., Bowles R.L.
A simple analytic 3-Dimensional Downburst model based on boundary layer stagnation flow
NASA Langley Research Center, Hampton, VA, NASA-TM-100632, (1988)

[9] Proctor F.H.
Terminal Area Simulation System
NASA Contractor report 4047, (April 1987)

[10] B. Cantaloube, T.H. Le
Modelisation de cisaillement de vent
Rapport ONERA n° 19/3619 SY

[11] D. Guffond
Etude de la cinematique des gouttes de pluie dans un cisaillement de vent
Rapport ONERA n° 16/3619 SY (1991)

[12] Dolfi A.
Système lidar à 2µm pour la détection des micro-rafales
Rapport ONERA RT 15/3619 SY, (Octobre 1992)

[13] Jones D.M. A. and Sims A. L.
Climatology of instantaneous rainfall rates
Journal of applied meteorology, Vol 17, (August 1978)

[14] Roys, G.P. and Kessler, E
Measuments by aircraft of condensed water in great plains thunderstorms
National severe storms laboratory publications. TN-49-NSSP-19, (1966)

[15] Melson W., Edward Jr.
Observation and comparison of rainfall measured at a high sample rate
Proceedings of the American meteorological society, 71st annual meeting, January 13-18, 1991, New Orleans (1991)

[16] Dan D. Vicroy
The aerodynamic effect of heavy rain on airplane performance
AIAA-90-3131-CP, (1990)

[17] D.J.Dunham, R.E Dunham Jr. and Gaudy M. Bezos
A summary of NASA Research on Effects of Heavy Rain on Airfoils
AGARD CP. 496, (May 1991)

[18] B.A. Campbell and G. M. Bezos
Steady-state and transitional aerodynamic characteristics of a wing in simulated heavy rain
NASA TP 2932, (August 1989)

[19] Anon, FAA Technical Standard Order
Airborne Windshear Warning and Escape Guidance Systems for Transport Airplanes
FAA TSO-C117, (July 1990)

Tables

	Configuration	Mass (Kg)
Generic transport aircraft A1	Take-off	137 000
	Landing	120 000
Three engines Medium range A2	Take-off	81 650
	Landing	60 840
Twin engines Long range A3	Take-off	210 000
	Landing	175 000
Four engines Long range A4	Take-off	260 000
	Landing	180 000

Table 1: Aircraft mass caracterictics

Landing configuration	A1	A2	A3	A4
wing loading (kg/m2)	461	420	481	501
Max thrust/ weight	0,31	0,29	0,28	0,26
Vref	135kt	142kt	141kt	141kt
Vref/Vs1g	1,31	1,40	1,28	1,28
Time engine response τ (s)	complete dynamic response ($\tau \approx 3s$)	3s	6s	4s

Table 2

XDB	Microburst wind field		
	t = 800s	t = 1000s	t = 1200s
- 3000 m	overshoot the runway $H0_{final}$=80m	too high final sink rate > 5m/s	final approach above the glide path
- 1500 m	Crash at X0=-1298m	Stall angle at X0= -1229m	overshoot the runway $H0_{final}$=51m

Table 3: Microburst location and time dispersal effect on the generic aircraft model in a penetrating approach.

Xdb	Go-around altitude	A2	A3	A4
-3000m	132m	87m	69m	78m
-1500m	72m	18m	Crash	Crash

Table 4: Aircraft model effect on minimum altitude during aborted landing. Dry microburst at t=800s

Figures

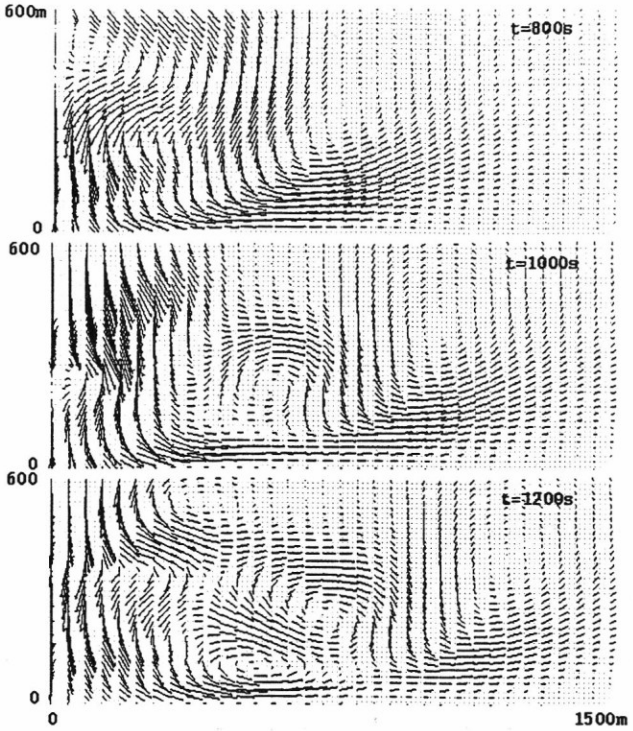

Fig 1. ONERA axisymmetric microburst model. Wind vector field at time t=800s, t=1000s, t=1200s.

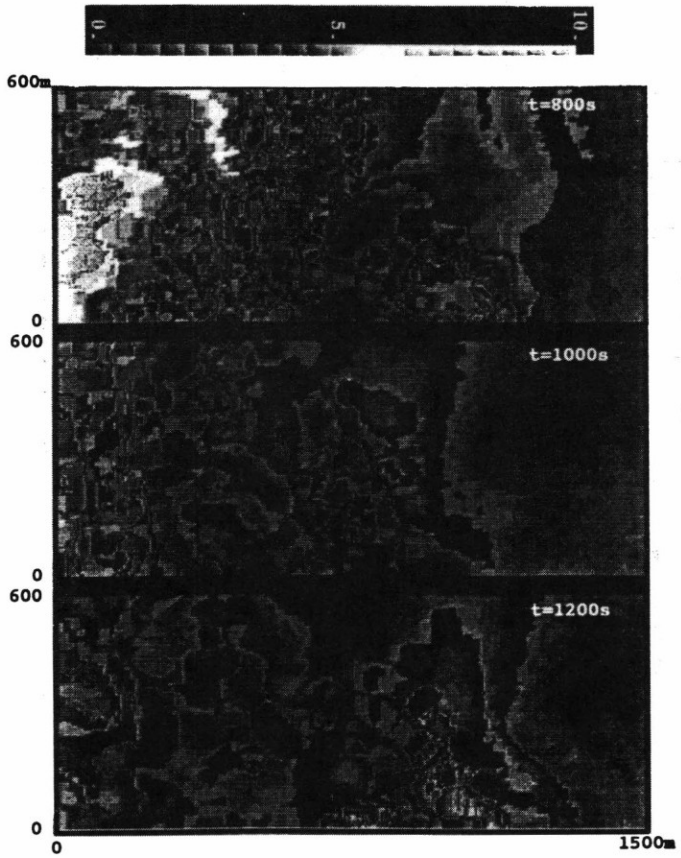

Fig 2. ONERA axisymmetric m: :roburst model. Rainfall rate coefficient at time t=800s, t=1000s, t=1200s.

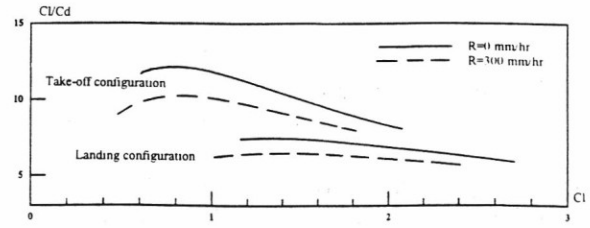

Fig 3. Rainfall effect on the drag polar related to the configuration (generic aircraft)

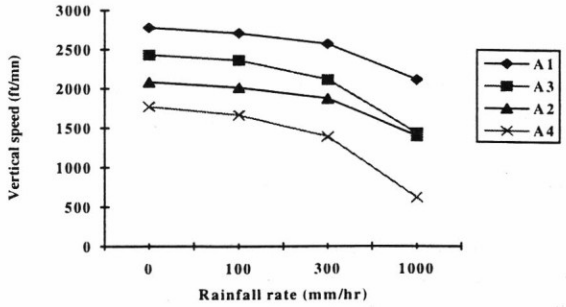

Fig 4. Rainfall effect on the climb performance in take-off configuration

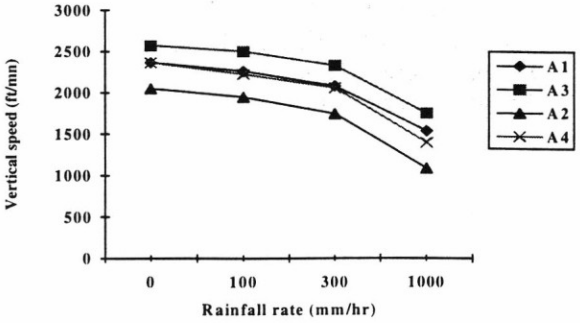

Fig 5. Rainfall effect on the climb performance in landing configuration

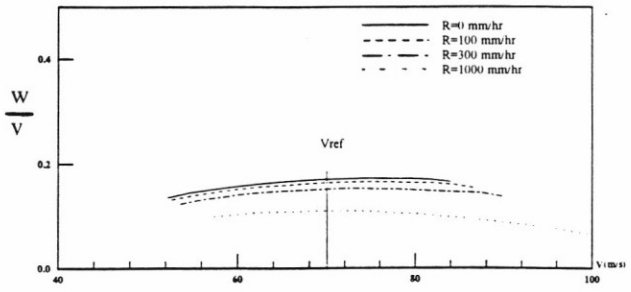

Fig 6. Rainfall effect on the specific excess power in a landing configuration (generic aircraft)

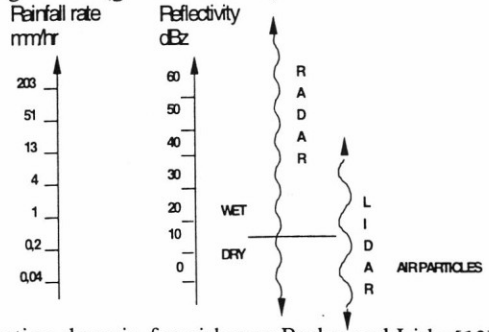

Fi: 7.Application domain for airborne Radar and Lidar[12]

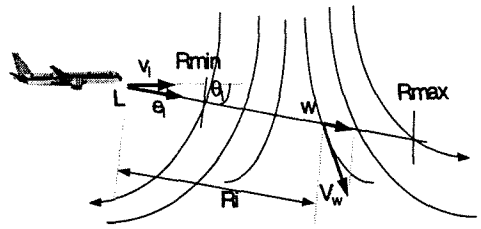

Fig 8. Lidar measurement

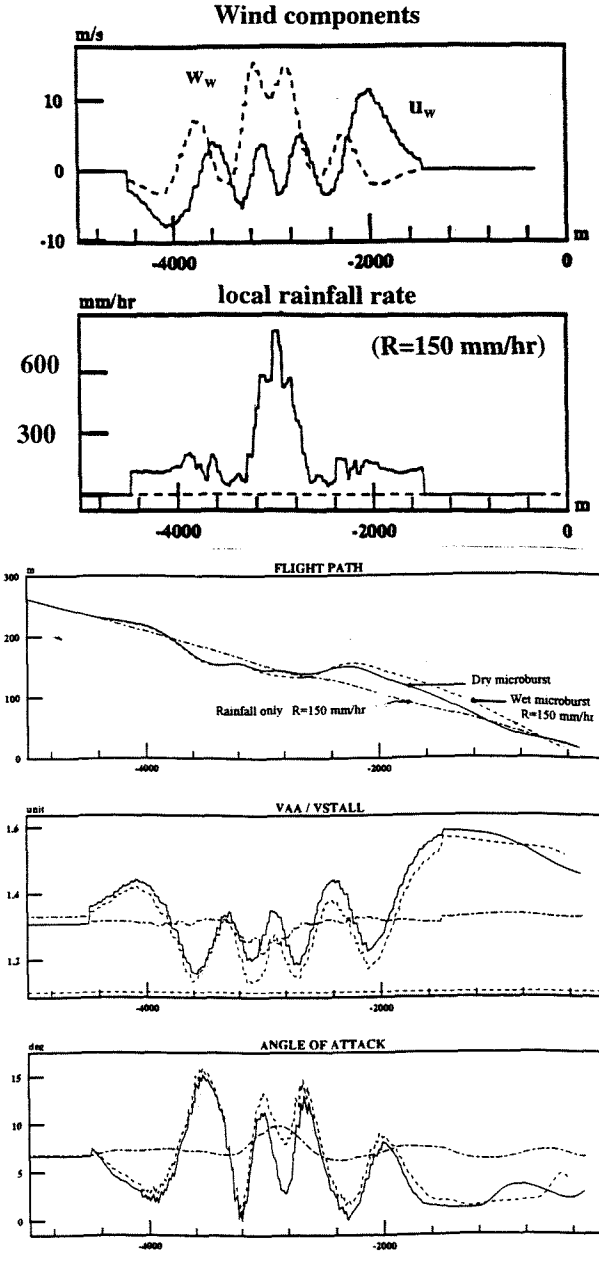

Fig 9 Generic aircraft on penetrating landing. Adverse environment parametric study (microburst at time t=1000s).

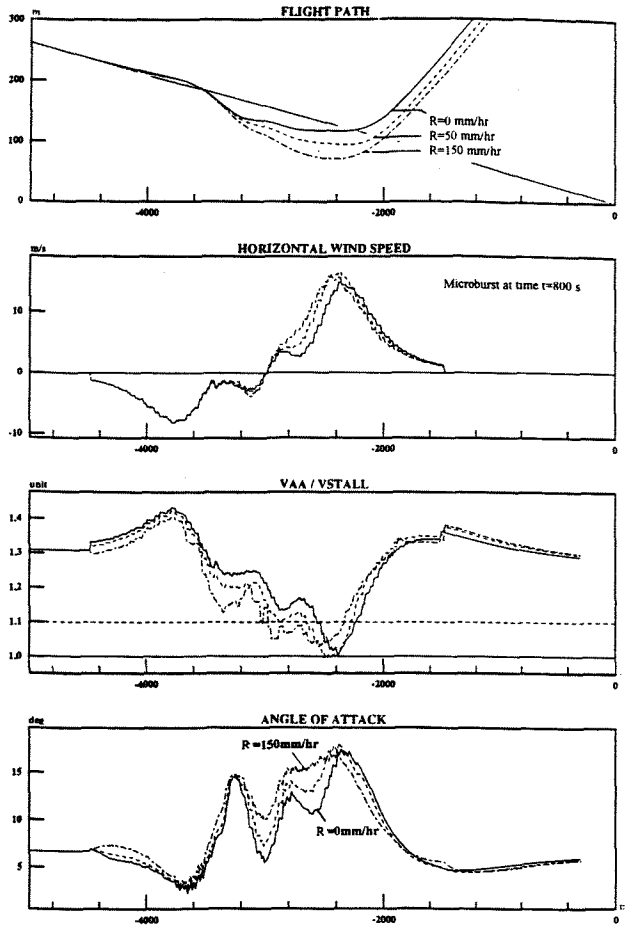

Fig 10. Generic aircraft on aborted approach. Rainfall effect (microburst at time t=800s).

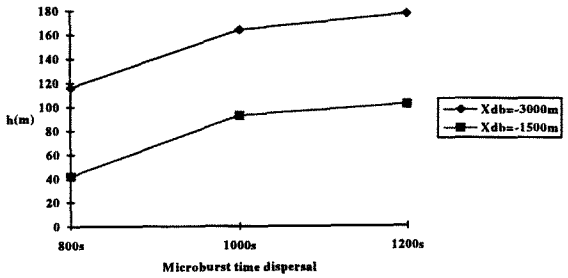

Fig 11. Microburst location and time dispersal effect on minimum altitude during aborted approach (generic aircraft model)

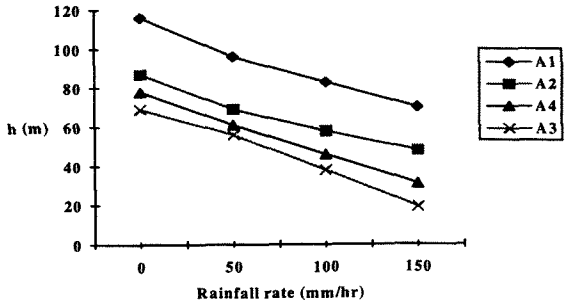

Fig 12. Minimum altitude during an aborted approach. Microburst located at 3000m ahead of runway threshold.

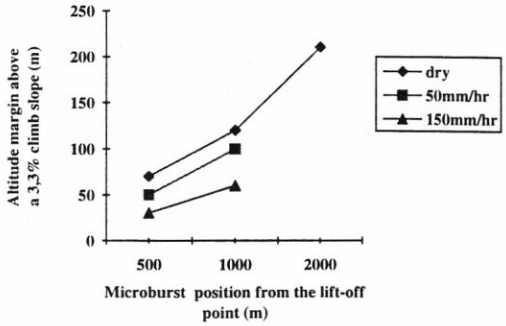

Fig13. Performance at take-off of the generic aircraft.

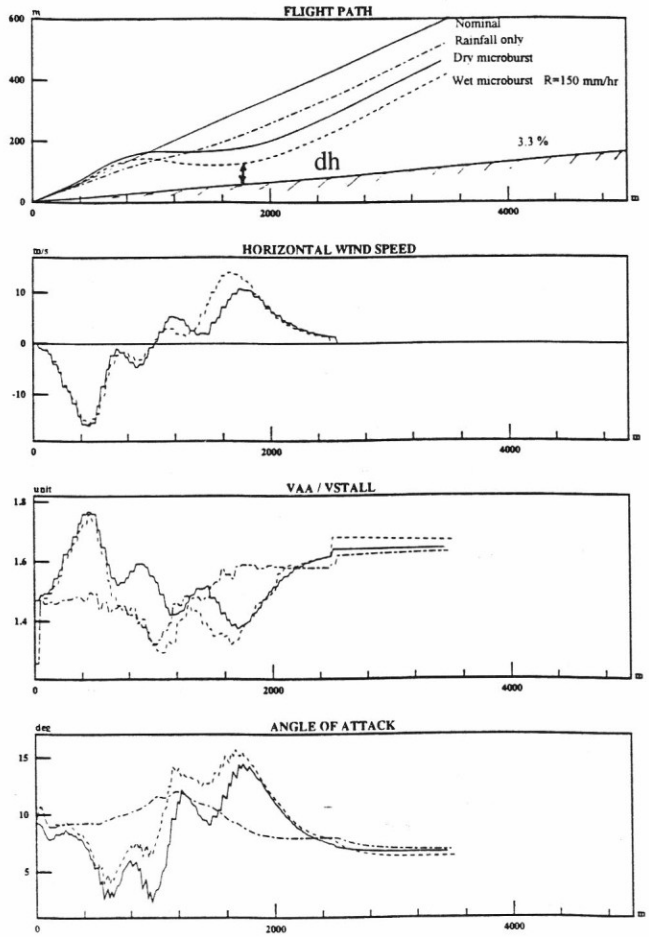

Fig 14. Generic aircraft at take-off. Adverse environment parametric study.

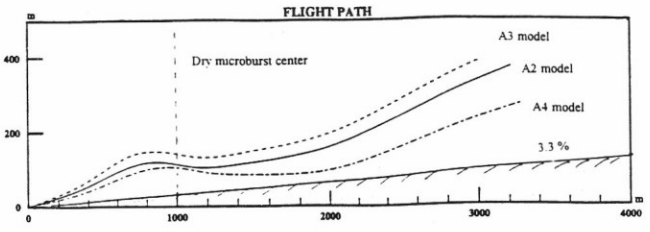

Fig 15. Aircraft parametric study at take-off. Microburst at t=800s centered at 1000m beyond lift off position.

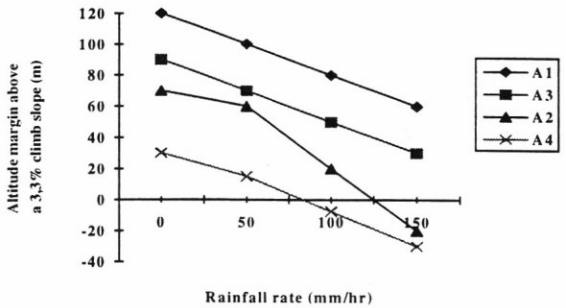

Fig 16. Rainfall effect at take-off. Microburst centered at 1000m beyond lift off position.

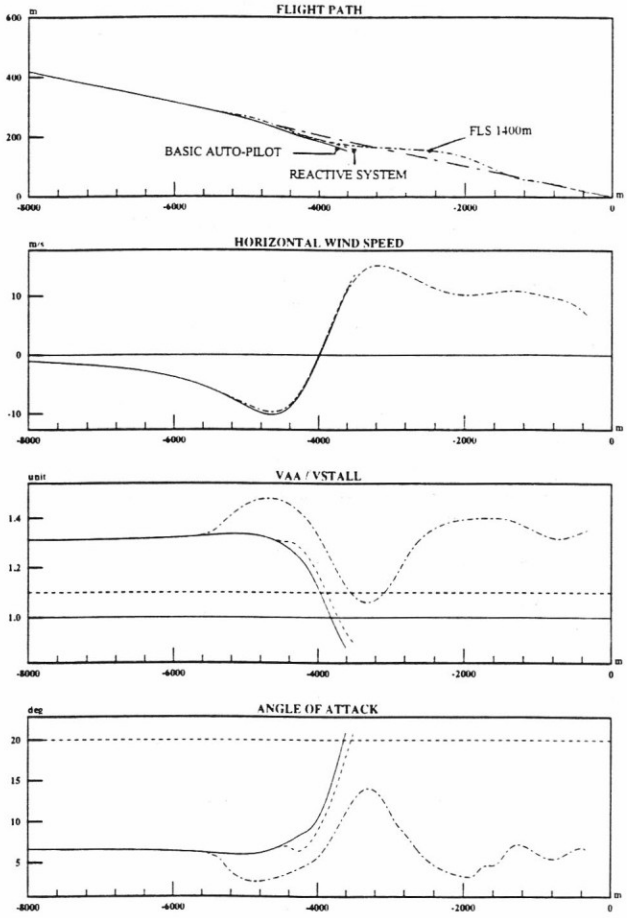

Fig 17. Comparison between various flight control systems during a penetrating landing

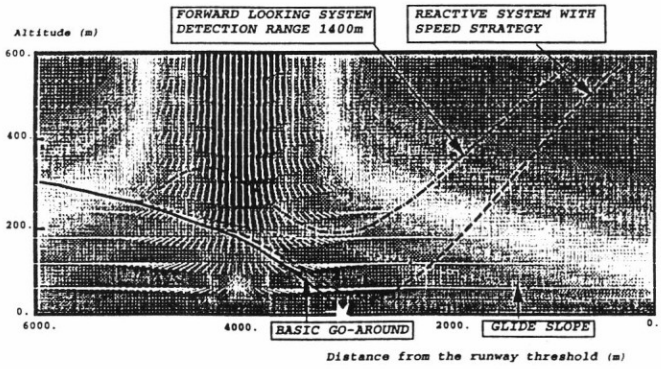

Fig 18. Comparison between various flight control systems during an aborted approach (flight path)

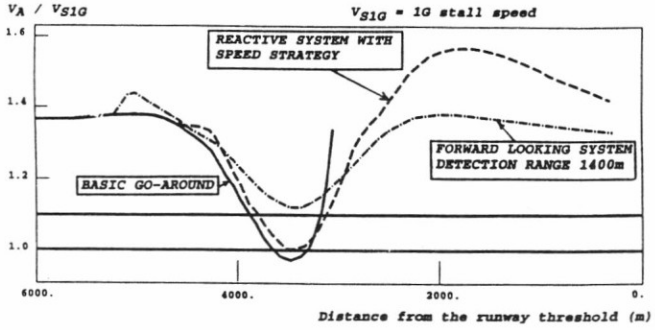

Fig 19. Comparison between various flight control systems during an aborted approach (Airspeed)

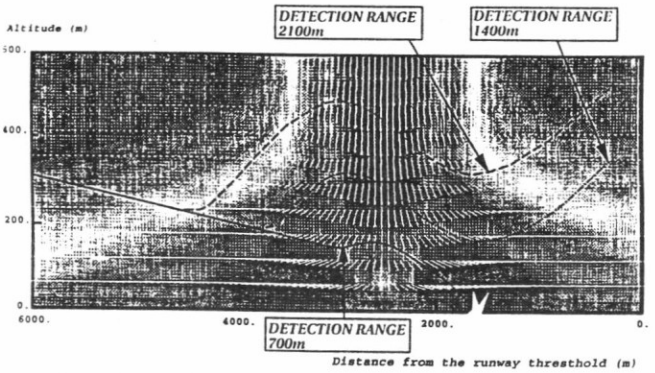

Fig 20. Effect of the maximum detection range during an aborted approach

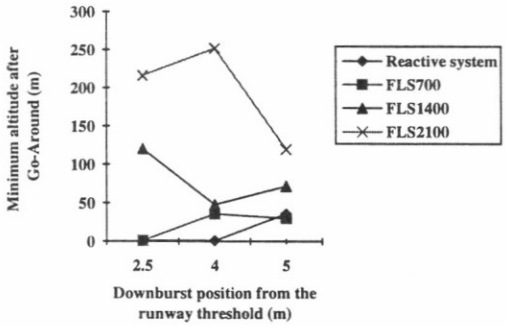

Fig 21. Comparison between various flight control systems during aborted landing (A4 model)

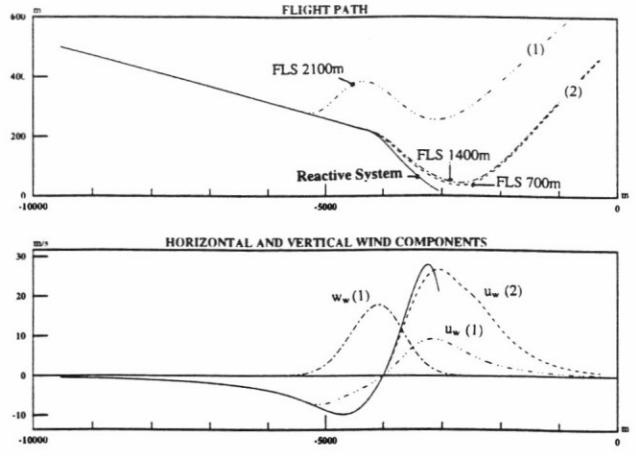

Fig 22. Comparison between various flight control systems during aborted landing (A4 aircraft model, XDB=4000m)

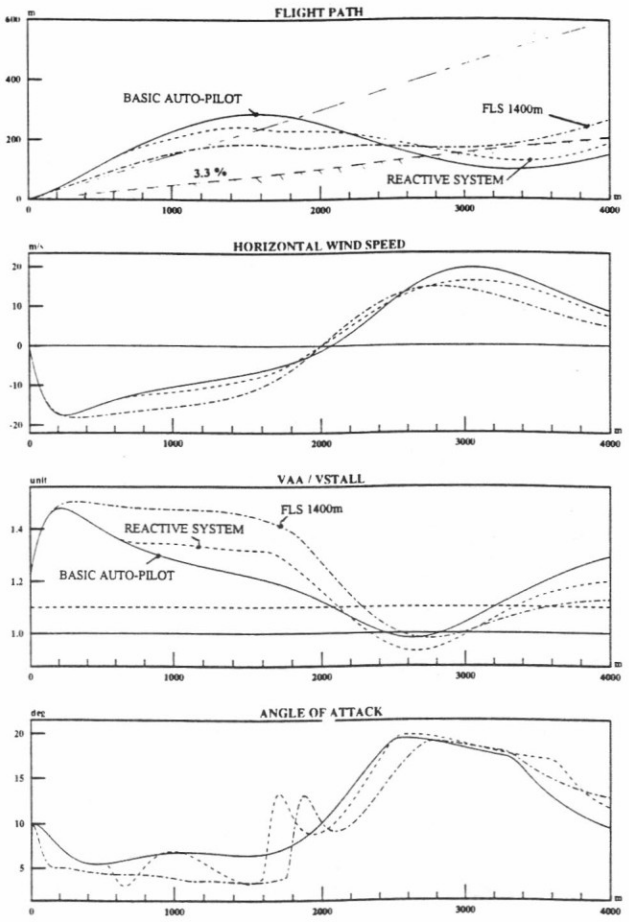

Fig 23. Comparison between various flight control systems during take-off (A3 model)

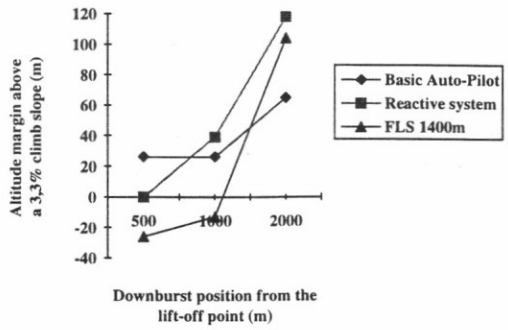

Fig 24. Comparison between various flight control systems at Take-off (generic aircraft model)

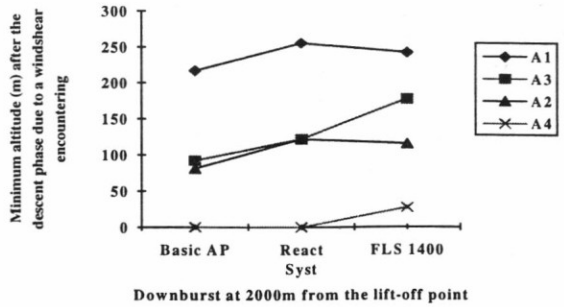

Fig 25. Aircraft parametric study at take-off. Comparison between systems